Biomass Burning Aerosol Radiative Effects in the Southeast Atlantic Depend Strongly on Meteorological Forcing Method

Eric Giuffrida et al

1 Smoke Evaluation

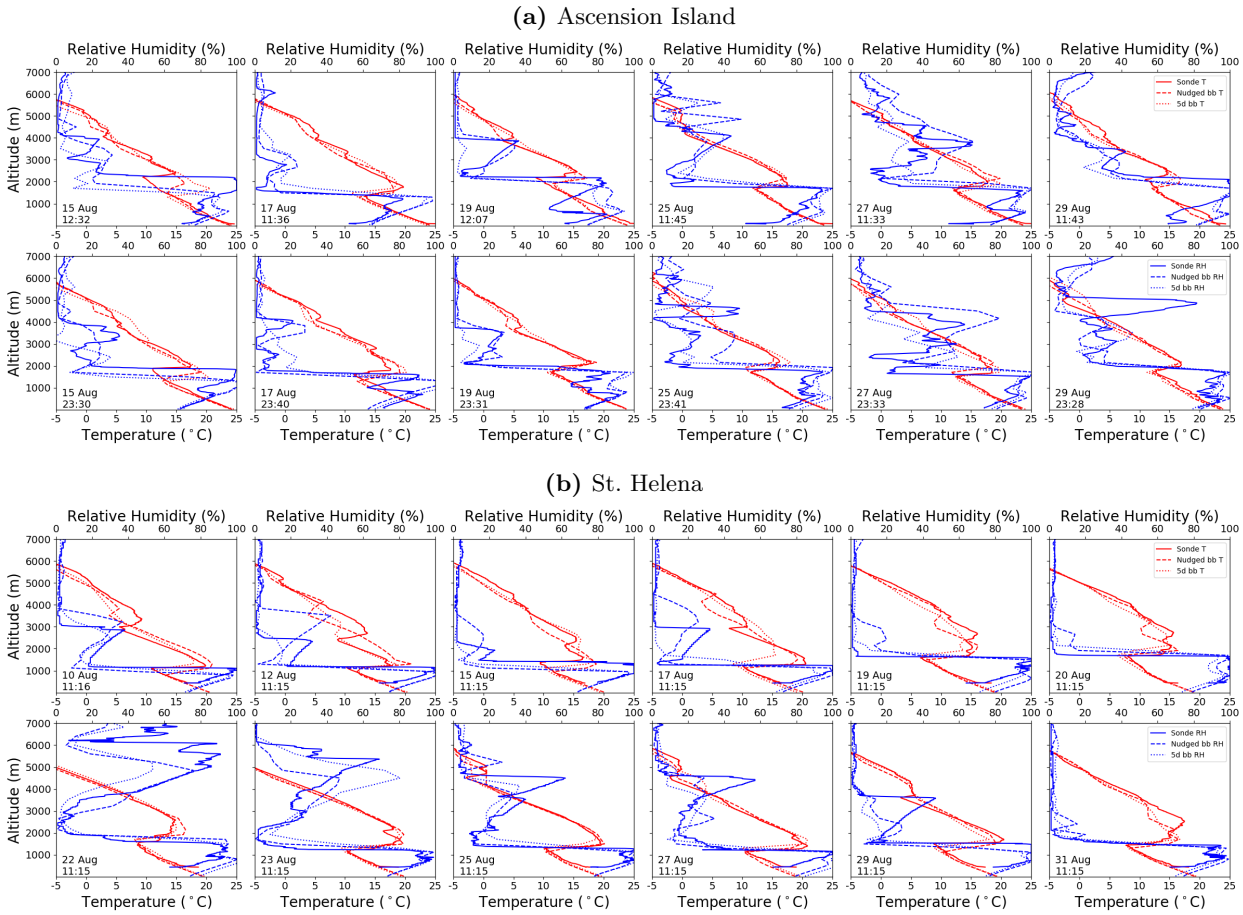

Figure S1: Vertical profiles of temperature (red) and RH (blue) for a sample of individual radiosonde launches (solid) compared to the corresponding Nudged$_{bb}$ (dashed) and 5d$_{bb}$ (dotted) simulated profiles at a) Ascension Island and b) St. Helena. Model values are derived by linear interpolation to match the location and time of the radiosondes. The date and time of each sonde release is shown on the bottom left. For Ascension Island, the sample days chosen are based on the time periods of major smoke events, 01 Aug to 20 Aug, and 21 Aug to 08 Sept, during both day and night times. For St. Helena, radiosondes were only available during daytime, so additional representative days were included.

2 Free Run Meteorology Evaluation

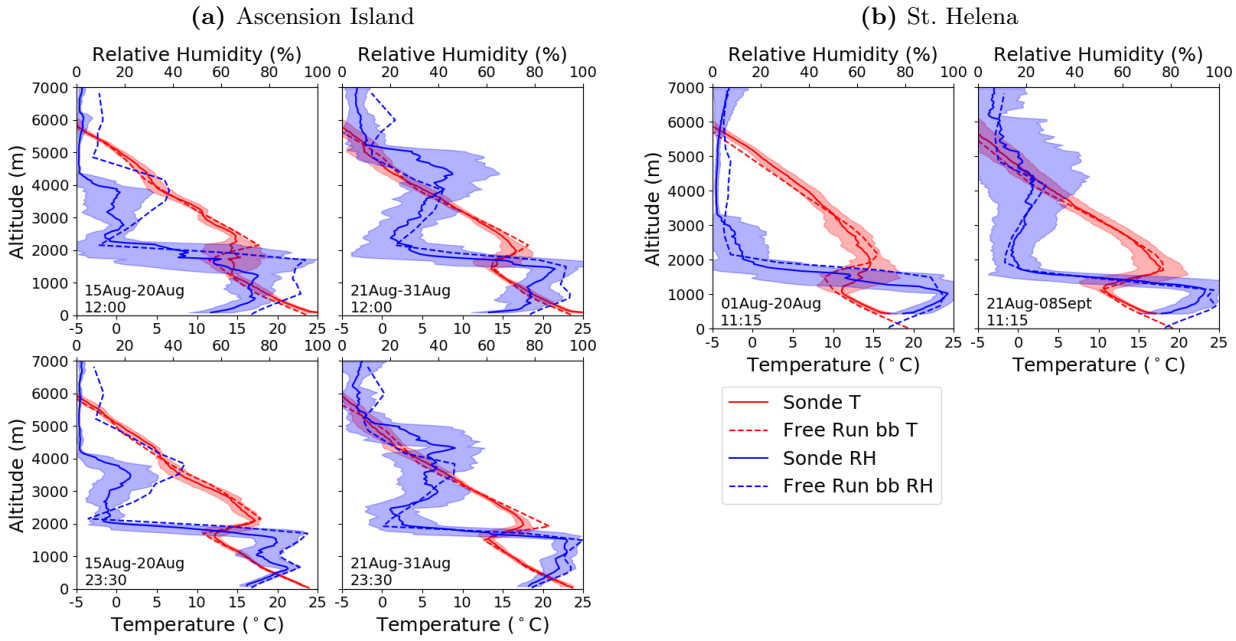

Figure S2: Mean vertical profiles of temperature (red) and RH (blue) from radiosondes launched within 01 Aug to 20 Aug (left column), and 21 Aug to 08 Sept (right column) at midday (top row) and midnight (bottom row) from a) Ascension Island and b) St. Helena. Corresponding Free Run$_{bb}$ (dashed) simulated values are derived by linear interpolation to match the location and time of the radiosondes (solid). Standard deviation among the individual radiosondes that make up each grouping are shaded red for temperature and shaded blue for RH. The date range and average launch time of the individual radiosondes that make up each grouping are shown on the bottom left.

(a) Ascension Island

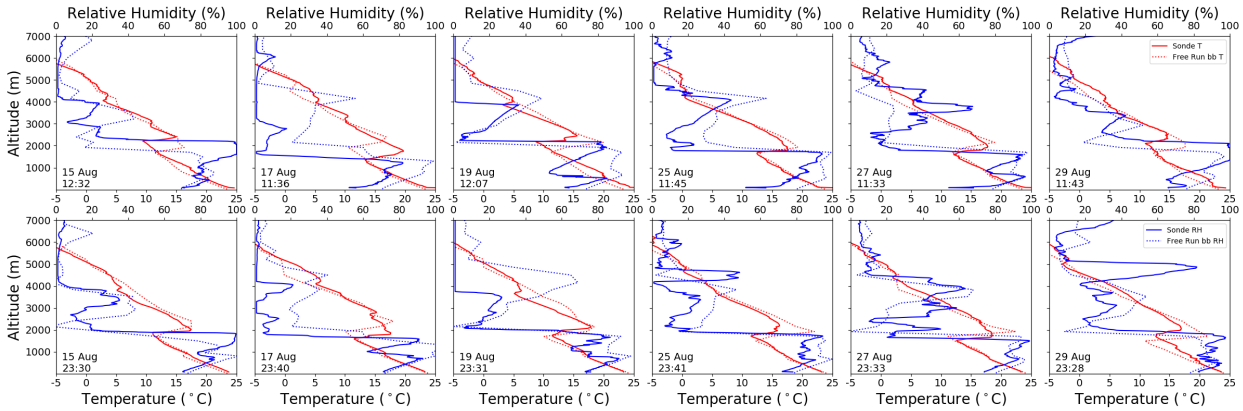

(b) St. Helena

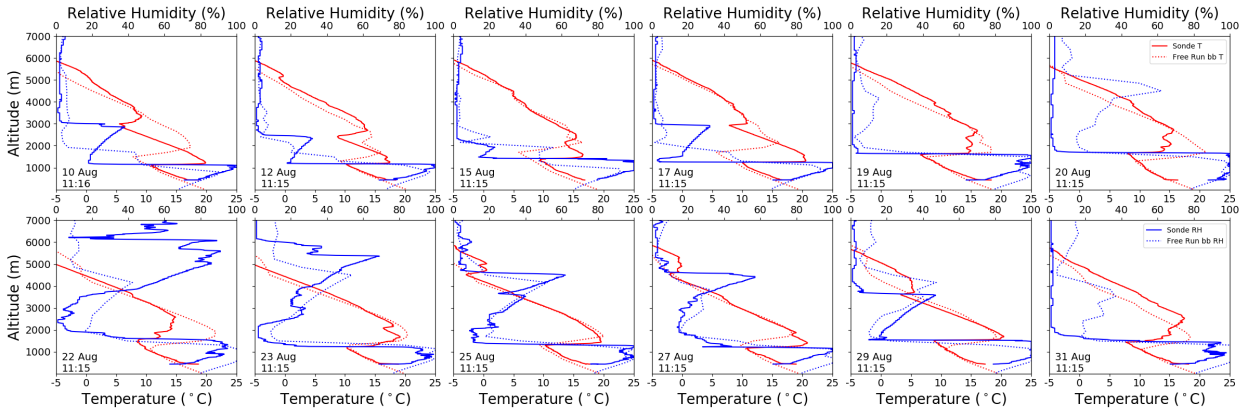

Figure S3: Vertical profiles of temperature (red) and RH (blue) for a sample of individual radiosonde launches (solid) compared to the corresponding Free Run$_{bb}$ (dotted) simulated profiles at a) Ascension Island and b) St. Helena. Model values are derived by linear interpolation to match the location and time of the radiosondes. The date and time of each sonde release is shown on the bottom left. For Ascension Island, the sample days chosen are based on the time periods of major smoke events, 01 Aug to 20 Aug, and 21 Aug to 08 Sept, during both day and night times. For St. Helena, radiosondes were only available during daytime, so additional representative days were included.

3 Cloud Evaluation

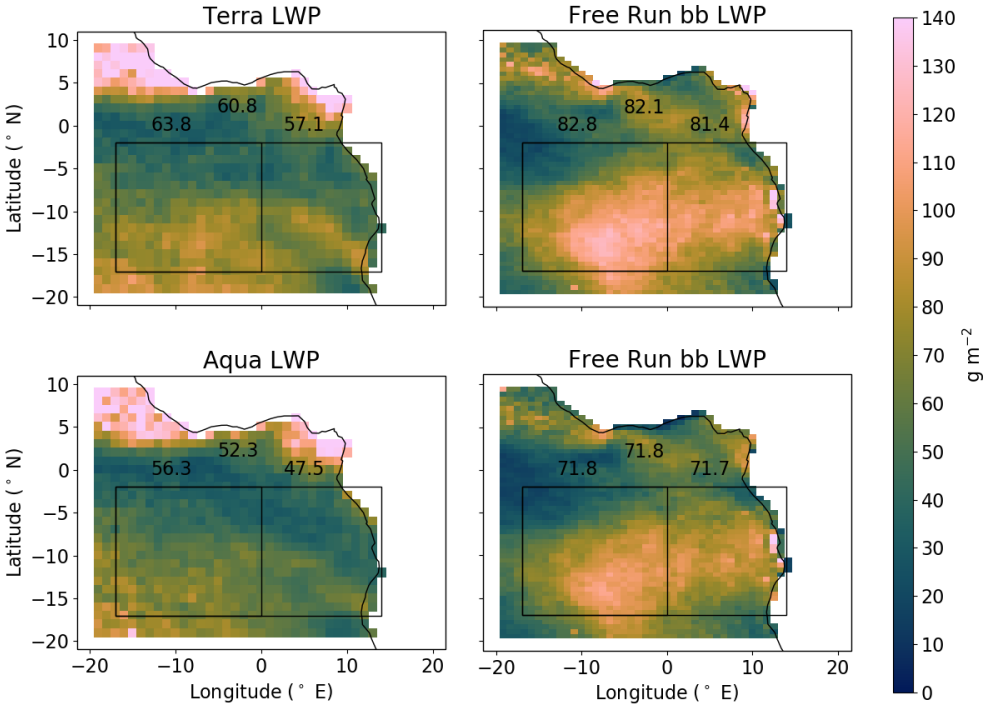

Figure S4: Mean LWP from 01 Aug to 08 Sept 2017 compared between MODIS and the Free Run$_{bb}$ simulation for both Terra (top row) and Aqua (bottom row) satellites. Values are means at the time of the satellites passing, approximately 10:30 UTC for Terra and 13:30 UTC for Aqua. Note MODIS includes convective clouds between 0 and 10° N that likely have large uncertainties in their LWP retrievals due to ice content. Clouds diagnosed from the model's convection parameterization are excluded from the model plots. Values printed are spatial averages of the overall (top), remote (left), and coastal (right) domains.

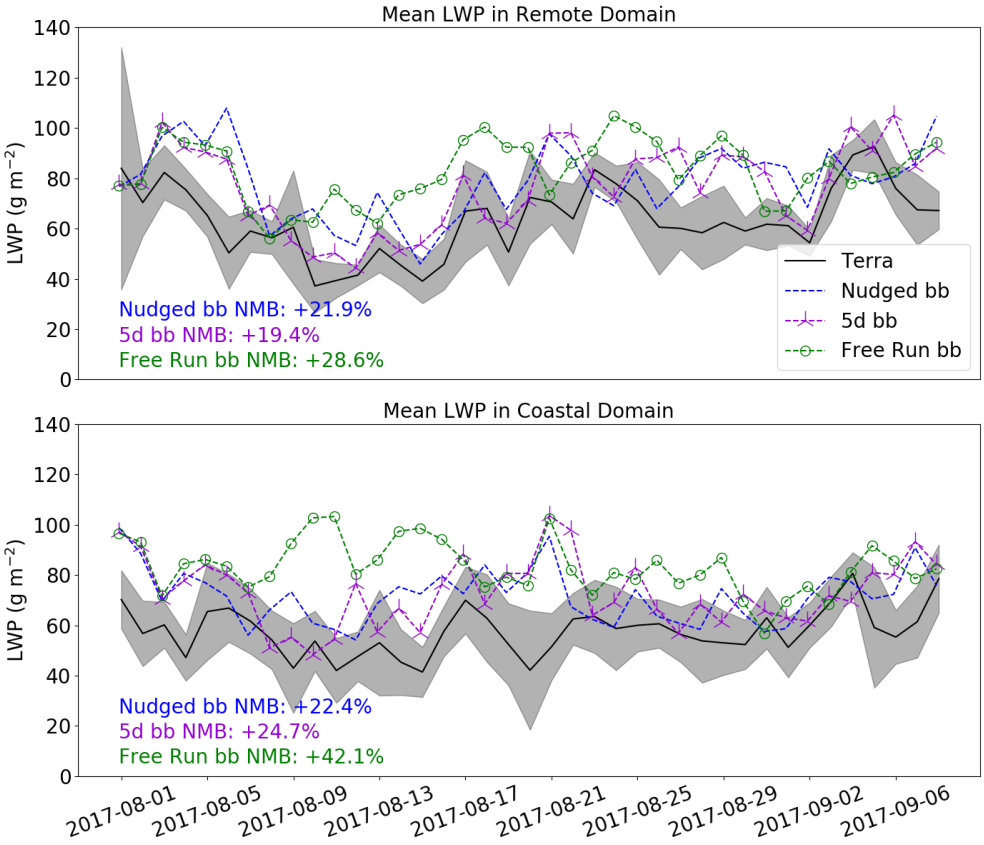

Figure S5: Time series of domain mean LWP as captured by Terra (black), the Nudged$_{bb}$ (blue), 5d$_{bb}$ (purple), and Free Run$_{bb}$ (green) simulations in the remote (top) and coastal (bottom) domains. Terra values are taken at approximately 10:30 UTC, with all data values less than zero removed. The grey shading shows the standard deviation around the L3 MODIS retrievals. Model values are taken at 10:30 UTC by linear interpolation between the 9:00 and 12:00 UTC outputs.

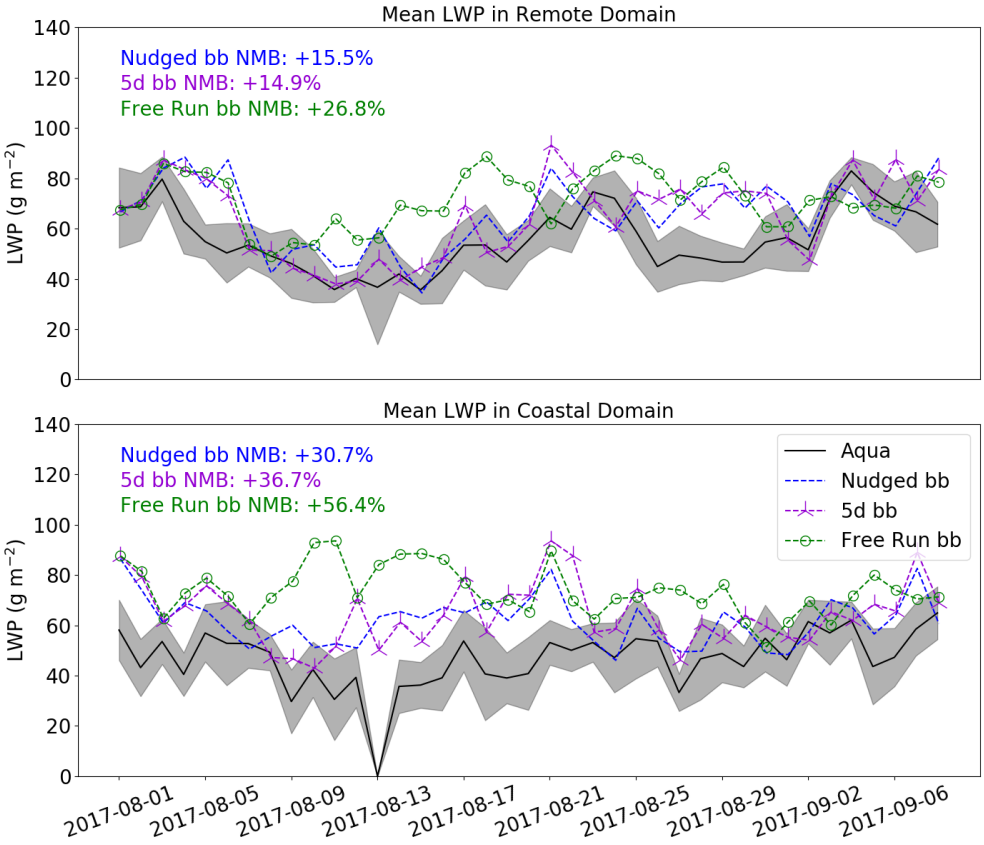

Figure S6: Time series of domain mean LWP as captured by Aqua (black), the Nudged$_{bb}$ (blue), 5d$_{bb}$ (purple), and Free Run$_{bb}$ (green) simulations in the remote (top) and coastal (bottom) domains. Aqua values are taken at approximately 13:30 UTC, with all data values less than zero removed. The grey shading shows the standard deviation around the L3 MODIS retrievals. Model values are taken at 13:30 UTC by linear interpolation between the bounding 12:00 and 15:00 UTC outputs.

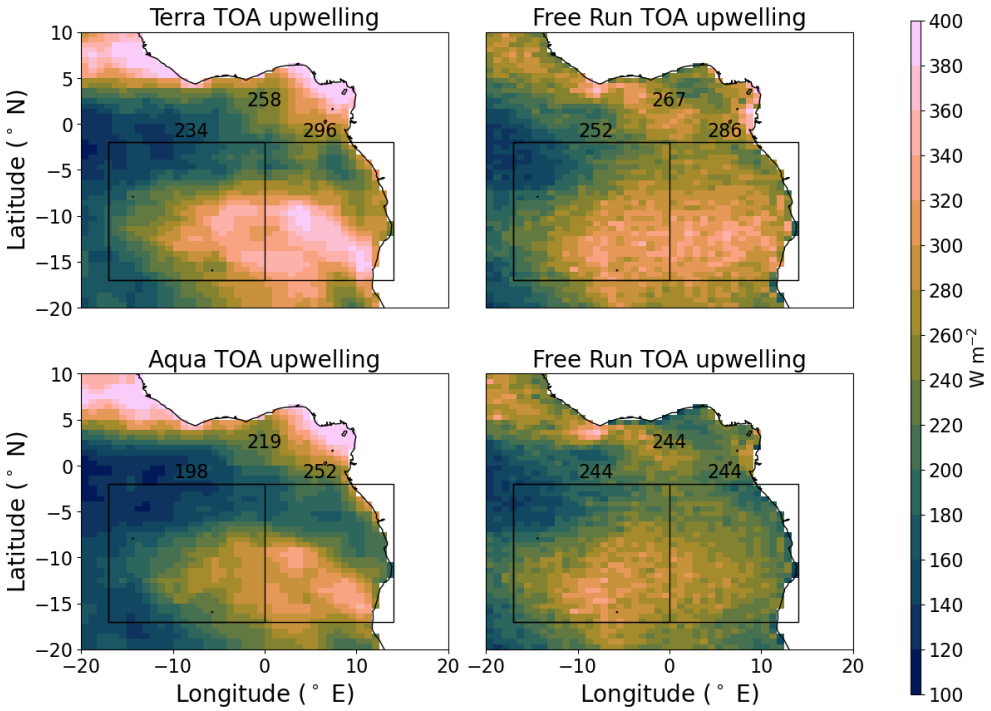

Figure S7: Mean SWout from 01 Aug to 08 Sept 2017 compared between CERES, and the Free Run$_{bb}$ simulation for both Terra (top) and Aqua (bottom) satellites. Values are the mean value at the time of the satellites passing, approximately 10:30 UTC for Terra and 13:30 UTC for Aqua. Values printed are spatial averages of the overall (top), remote (left), and coastal (right) domains.

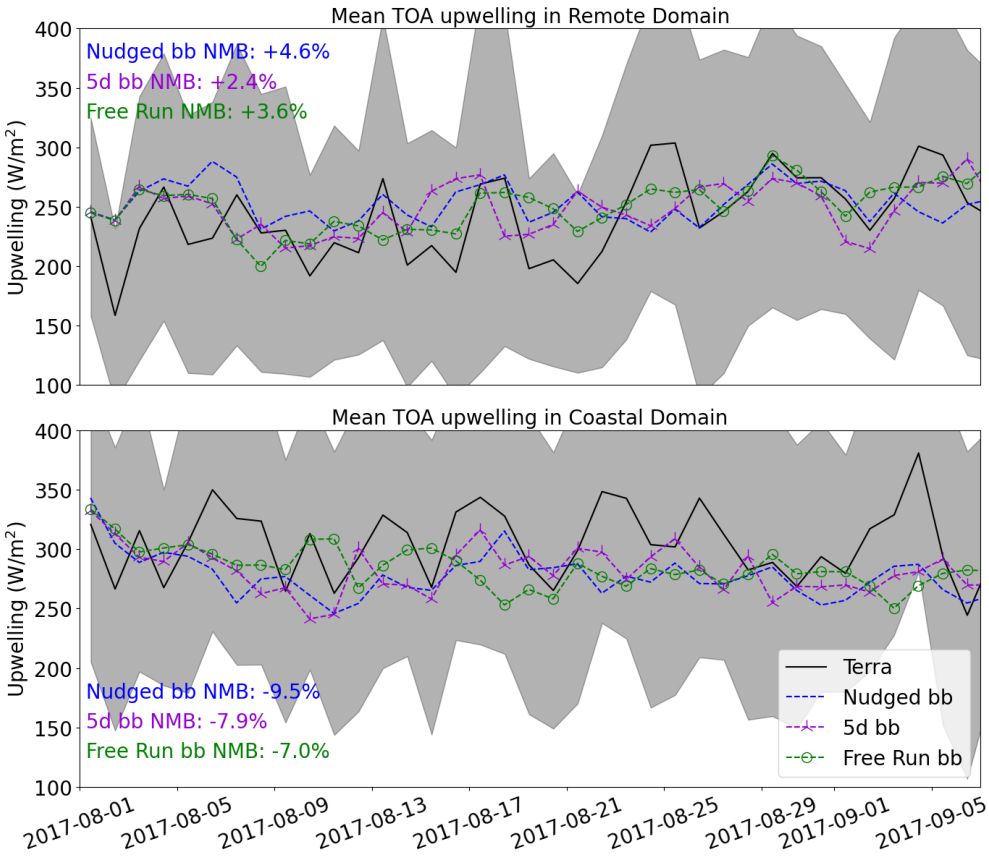

Figure S8: Time series of domain mean SWout as captured by Terra (black), the Nudged$_{bb}$ (blue), 5d$_{bb}$ (purple), and Free Run$_{bb}$ (green) simulations in the remote (top) and coastal (bottom) domains. The grey shading shows the standard deviation around the CERES retrievals. Both Terra and model values are taken by averaging outputs between 9:00 and 12:00 UTC, as these times bound the satellite's overpass time of approximately 10:30 UTC.

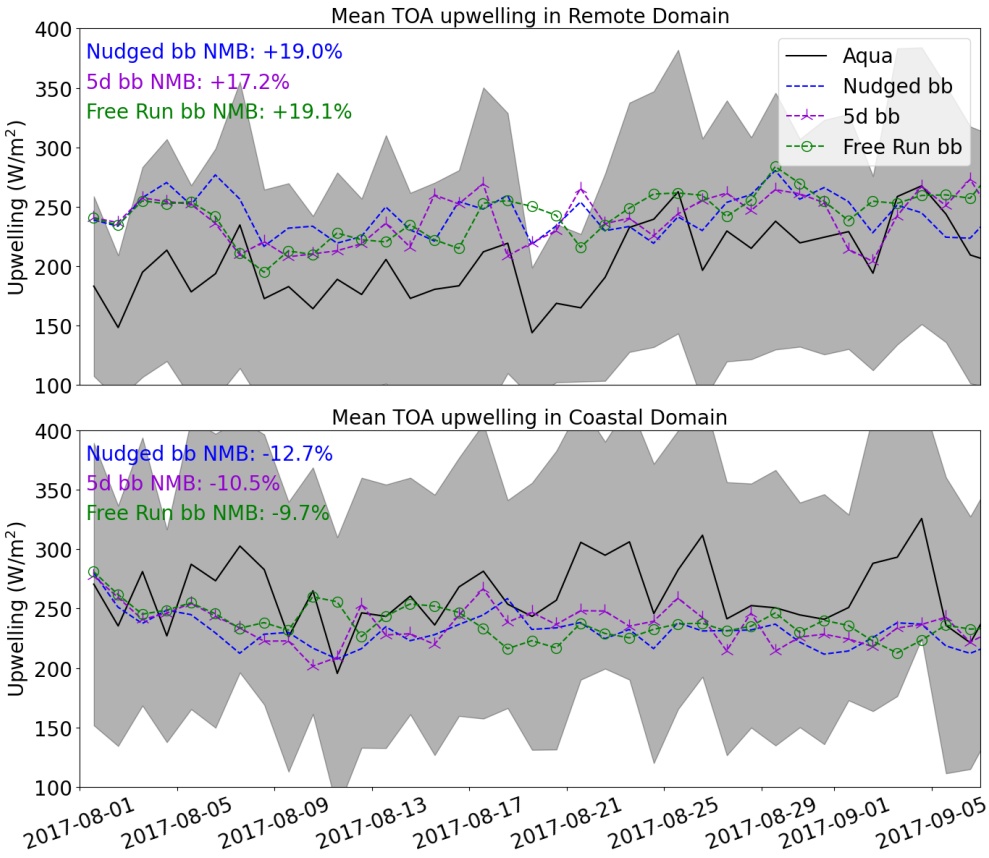

Figure S9: Time series of domain mean SWout as captured by Aqua (black), the Nudged$_{bb}$ (blue), 5d$_{bb}$ (purple), and Free Run$_{bb}$ (green) simulations in the remote (top) and coastal (bottom) domains. The grey shading shows the standard deviation around the CERES retrievals. Both Aqua and model values are taken by averaging outputs between 12:00 and 15:00 UTC, as these times bound the satellite's overpass time of approximately 13:30 UTC.

4 Free Run Smoke Evaluation

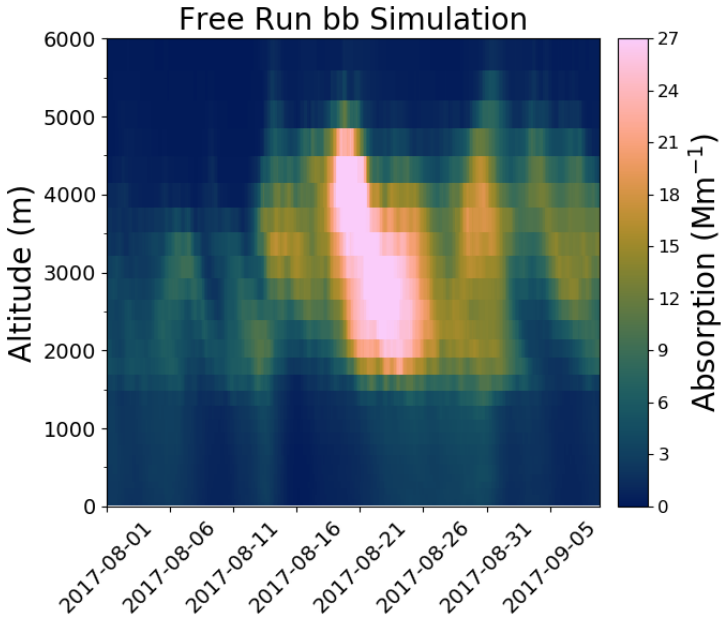

Figure S10: Time series of absorption coefficient in the remote domain for the Free Run$_{bb}$ simulation.

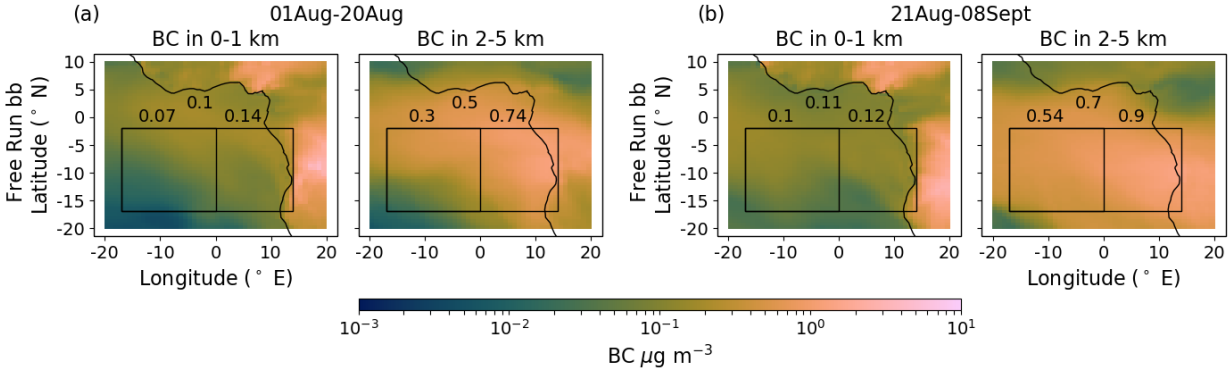

Figure S11: BC mass concentrations for the Free Run$_{bb}$ simulation averaged over the two major smoke episode time periods, 01 Aug to 20 Aug (a) and 21 Aug to 08 Sept (b), 2017. Mass concentrations are averaged from 0-1 km (left column) and 2-5 km (right column) to show within and above the MBL respectively. Values printed are spatial averages of the overall (top), remote (left), and coastal (right) domains.

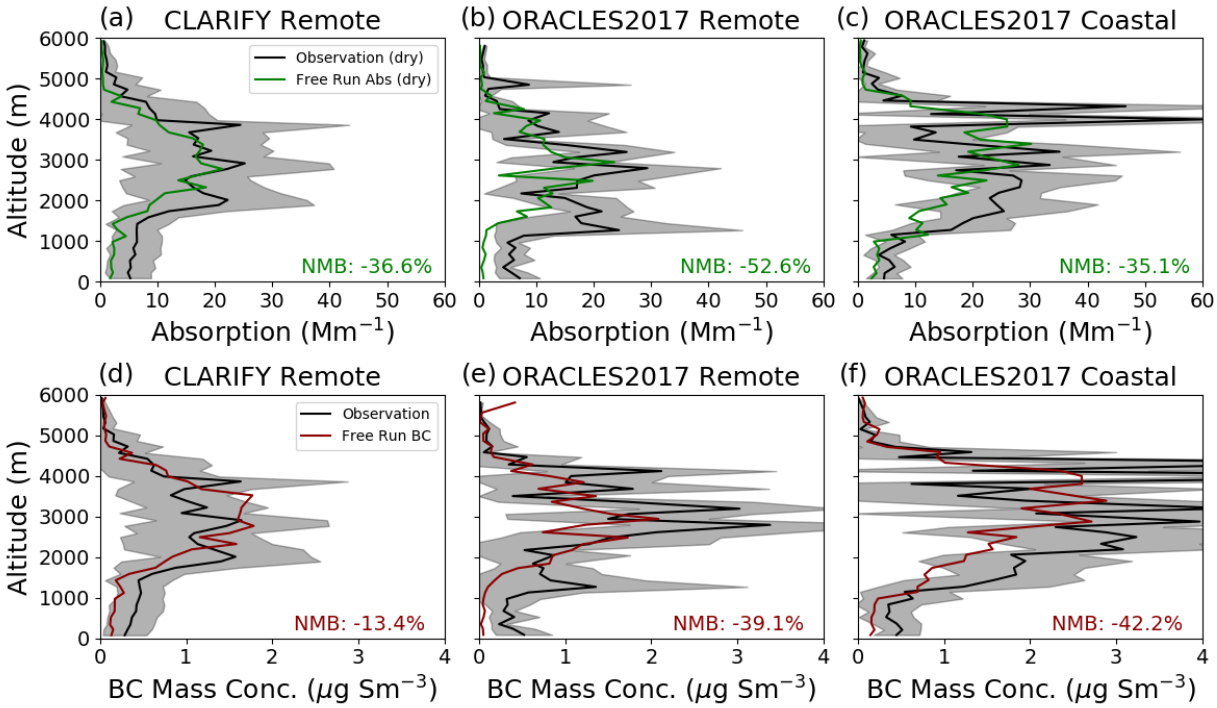

Figure S12: Absorption coefficient (green) and BC mass concentration (red) compared between Free Run$_{bb}$ (in color), and flight data (black) for the ORACLES2017 flights in the coastal domain (c, f), ORACLES2017 flights in the remote domain (b, e), and CLARIFY flights in the remote domain (a, d). The flight data is represented by 1 minute means omitting in-cloud data. Corresponding model values were captured using an interpolation algorithm to match UM grid locations to the flight path. The final plots were made using 150 m averages to reduce the noise. The standard deviation within these 150 m intervals for the flight data is shaded grey.

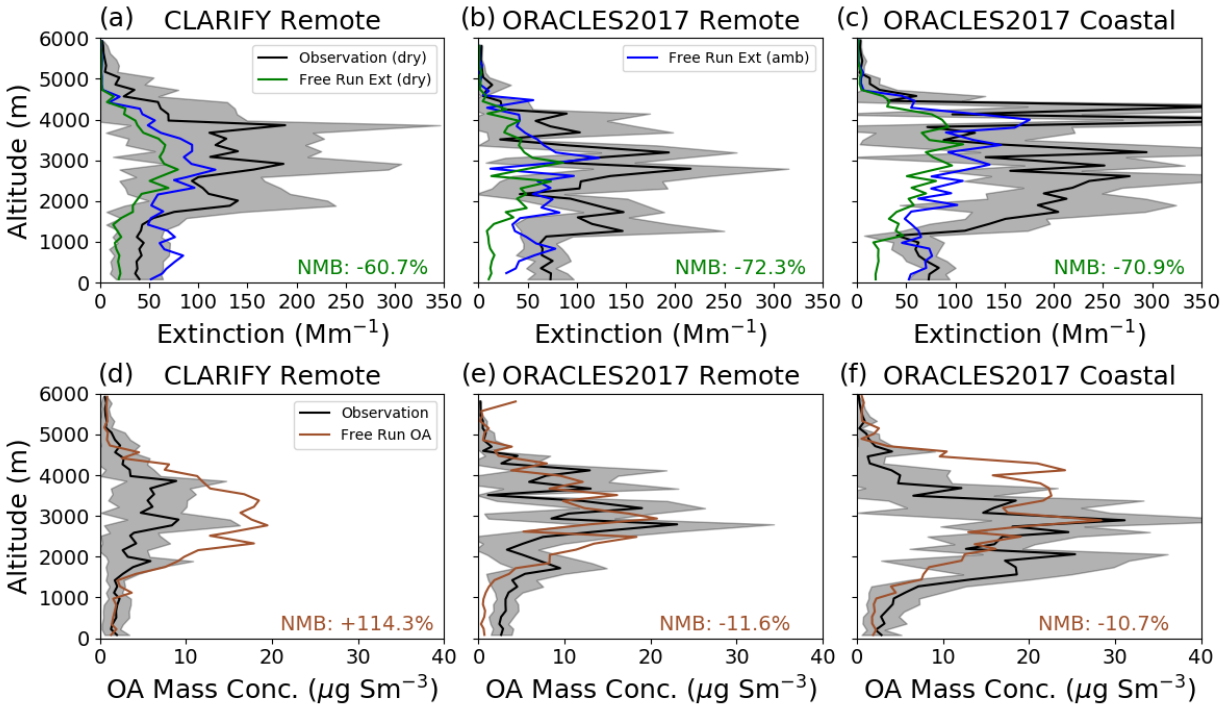

Figure S13: Extinction coefficient (green for dry, blue for ambient RH) and OA mass concentration (brown) compared between Free Run$_{bb}$ (in color), and flight data (black) for the ORACLES2017 flights in the coastal domain (c, f), ORACLES2017 flights in the remote domain (b, e), and CLARIFY flights in the remote domain (a, d). The flight data is represented by 1 minute means omitting in-cloud data. Corresponding model values were captured using an interpolation algorithm to match UM grid locations to the flight path. The final plots were made using 150 m averages to reduce the noise. The standard deviation within these 150 m intervals for the flight data is shaded grey.

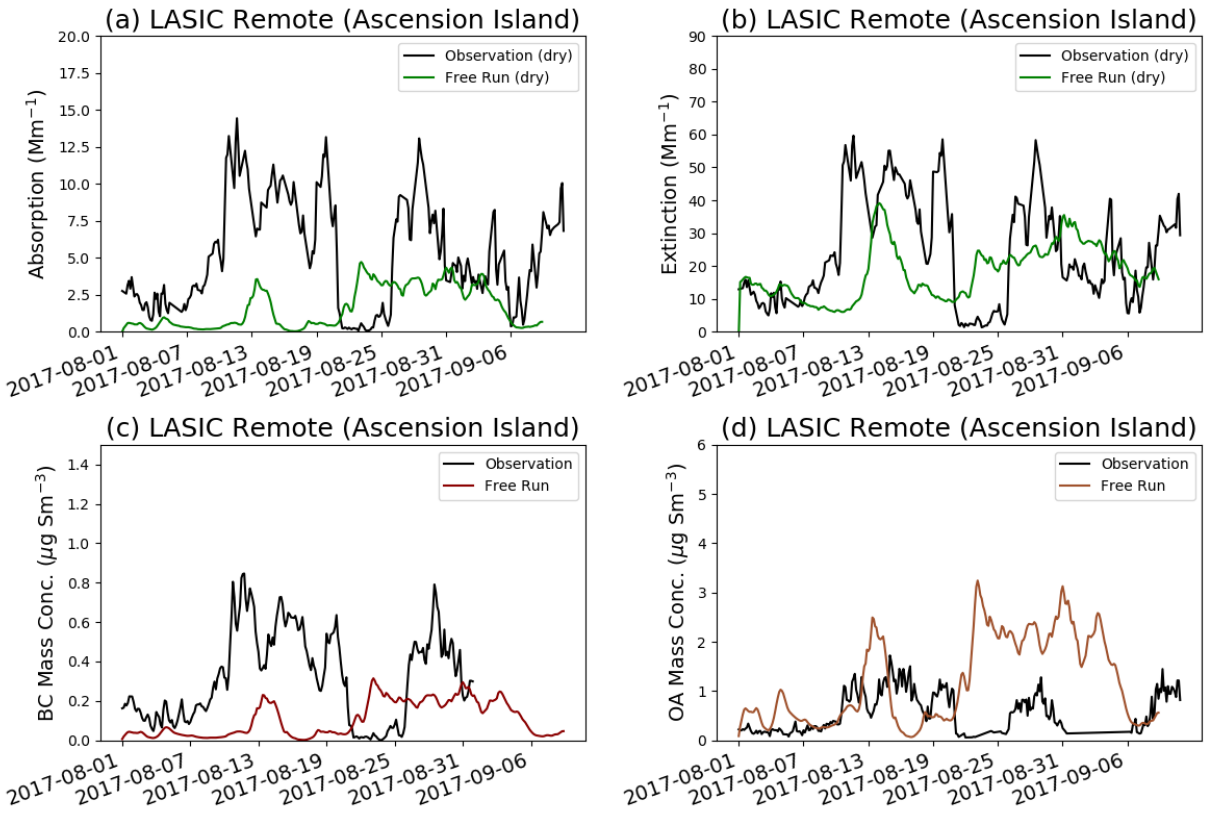

Figure S14: Dry absorption coefficient (a, green), dry extinction coefficient (b, green), BC mass concentration (c, red), and OA mass concentration (d, orange) compared between the Free Run$_{bb}$ (in color), and near surface Ascension Island measurements of LASIC (black). LASIC data is represented by three hourly means, with aerosols larger than 1.0 μm excluded from the absorption and extinction measurements. Model data is extracted at the location of the ARM Mobile Facility 1 of LASIC at a three hourly resolution.

5 DRE Scattering and Absorption

Table S1: DRE Scattering (W m^{-2}) averaged over each domain from 01 Aug to 20 Aug, 21 Aug to 08 Sept, and 01 Aug to 08 Sept, 2017.

	Domain	Nudged	1d	2d	5d	5dalt	Free Run
DRE Scattering (W m^{-2}) from 01 Aug to 20 Aug	Coastal	-5.3	-5.5	-5.2	-4.6	-4.2	-5.1
	Remote	-1.7	-1.6	-2.0	-1.7	-1.7	-1.1
	Overall	-3.4	-3.4	-3.5	-3.0	-2.9	-3.0
DRE Scattering (W m^{-2}) from 21 Aug to 08 Sept	Coastal	-10.7	-10.5	-9.6	-8.8	-8.6	-9.1
	Remote	-5.1	-4.1	-4.6	-4.0	-4.6	-5.3
	Overall	-7.7	-7.0	-6.9	-6.2	-6.4	-7.0
DRE Scattering (W m^{-2}) from 01 Aug to 08 Sept	Coastal	-7.9	-7.9	-7.4	-6.6	-6.5	-7.0
	Remote	-3.4	-2.8	-3.3	-2.8	-3.2	-3.2
	Overall	-5.5	-5.1	-5.2	-4.5	-4.7	-4.9

Table S2: DRE Absorbing (W m^{-2}) averaged over each domain from 01 Aug to 20 Aug, 21 Aug to 08 Sept, and 01 Aug to 08 Sept, 2017.

	Domain	Nudged	1d	2d	5d	5dalt	Free Run
DRE Absorbing (W m^{-2}) from 01 Aug to 20 Aug	Coastal	18.0	19.5	18.3	16.0	15.0	17.1
	Remote	4.8	5.1	5.3	4.1	4.1	3.3
	Overall	10.9	11.7	11.3	9.6	9.1	9.7
DRE Absorbing (W m^{-2}) from 21 Aug to 08 Sept	Coastal	28.8	29.0	27.8	27.2	26.3	24.9
	Remote	12.9	13.4	12.7	11.4	12.0	12.5
	Overall	20.2	20.6	19.6	18.6	18.6	18.2
DRE Absorbing (W m^{-2}) from 01 Aug to 08 Sept	Coastal	23.3	24.1	22.9	21.5	20.8	20.9
	Remote	8.7	9.1	8.9	7.7	8.2	7.8
	Overall	15.4	16.0	15.3	14.0	14.0	13.8

6 Indirect Radiative Effects

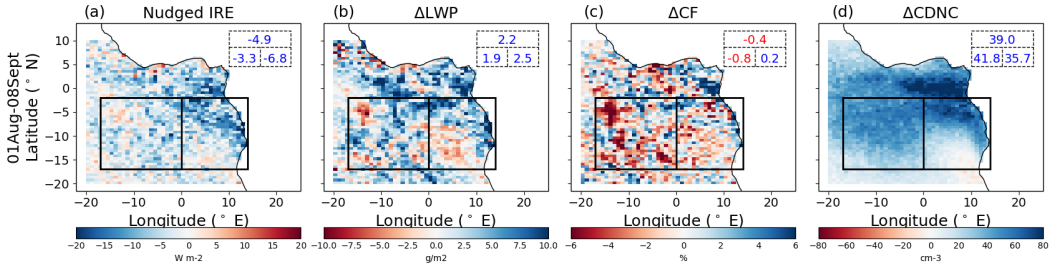

Figure S15: Nudged IRE (a) calculated according to Eq. (3), and averaged over the SEA from 01 Aug to 08 Sept, 2017. The corresponding changes in LWP (b), CF (c), and CDNC at cloud top (d) are calculated over the same time span across the simulations used in Eq. (3), *bbnoaa* and *nobbnoaa*. The difference between *bbnoaa* - *nobbnoaa* is represented above by Δ. Values in the top right corner represent spatial averages of the overall (top), remote (left), and coastal (right) domains in the respective units of each subplot. The subplots show good correlation between IRE and the changes in LWP, CF, and CDNC, with CDNC and LWP being the stronger drivers of the IRE. The CF subplot shows some of the slight warming areas of the IRE can be attributed to changes in cloud locations between *bbnoaa* and *nobbnoaa*. Although only nudged is shown, these findings hold true across all meteorological forcing techniques. LWP was calculated by integrating the liquid water content in each vertical column of grid cells. CF was calculated by taking the maximum value within the boundary layer. CDNC at cloud top was calculated by extracting model output CDNC at the highest grid cell within the boundary layer that contained a value greater than 0.00001 kg cloud water per kg air, and removing all cloud free data. All these variables were lastly time averaged to yield the above plots.

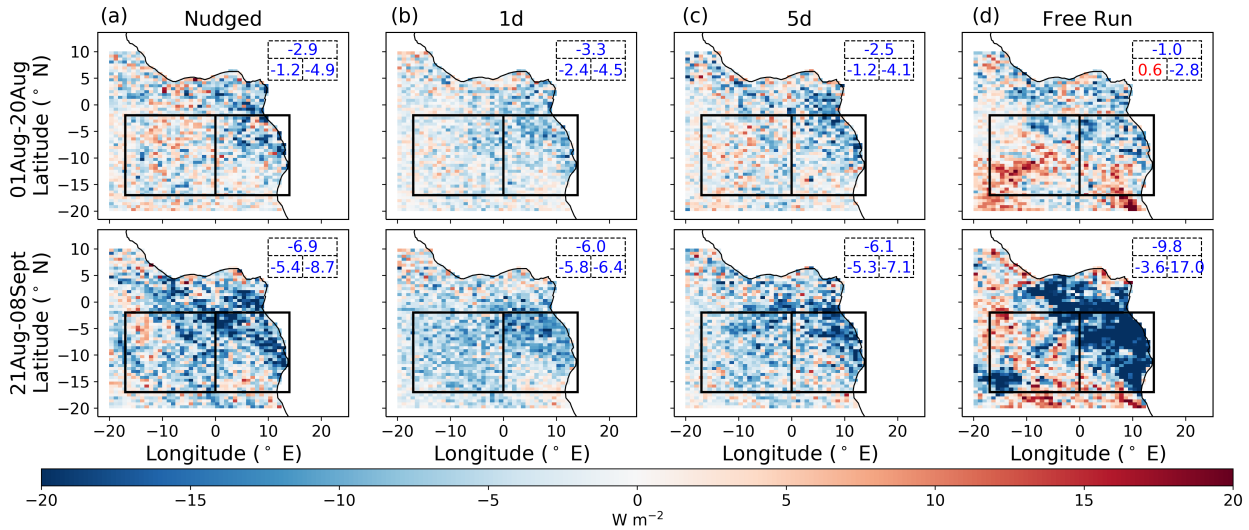

Figure S16: IRE calculated according to Eq. (3), and averaged over the SEA from 01 Aug to 20 Aug (top row), and 21 Aug to 08 Sept (bottom row), 2017, for the Nudged (a), 1d (b), 5d (c), and Free Run (d) simulation sets. Values in the top right corner represent spatial averages of the overall (top), remote (left), and coastal (right) domains. Positive mean magnitudes are red for warming, and negative are blue for cooling.

7 Semi-Direct Radiative Effect

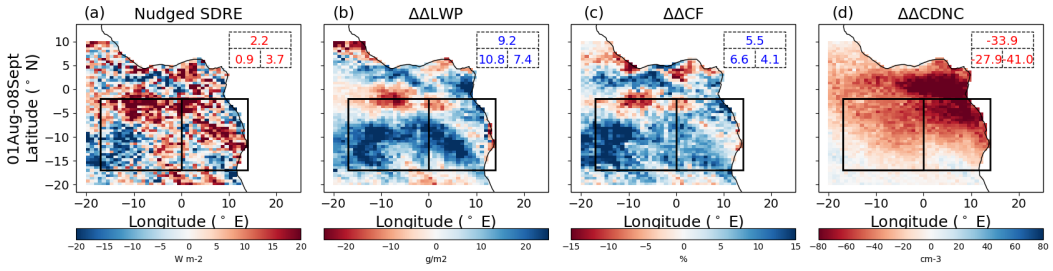

Figure S17: Nudged SDRE (a) calculated according to Eq. (4), and averaged over the SEA from 01 Aug to 08 Sept, 2017. The corresponding changes in LWP (b), CF (c), and CDNC at cloud top (d) are calculated over the same time span across the simulations used in Eq. (4), or the double difference of *bb* - *nobb* and *bbnoaa* - *nobbnoaa*. The double difference is represented above by ΔΔ. Values in the top right corner represent spatial averages of the overall (top), remote (left), and coastal (right) domains in the respective units of each subplot. The subplots show good correlation between SDRE and the changes in LWP, CF, and CDNC. The changes in LWP, CF, and CDNC that contribute to the SDRE are locally substantially larger than those contributing to the IRE (Fig. S15). Although only nudged is shown, these findings hold true across all meteorological forcing techniques. LWP was calculated by integrating the liquid water content in each vertical column of grid cells. CF was calculated by taking the maximum value within the boundary layer. CDNC at cloud top was calculated by extracting model output CDNC at the highest grid cell within the boundary layer that contained a value greater than 0.00001 kg cloud water per kg air, and removing all cloud free data. All these variables were lastly time averaged to yield the above plots.

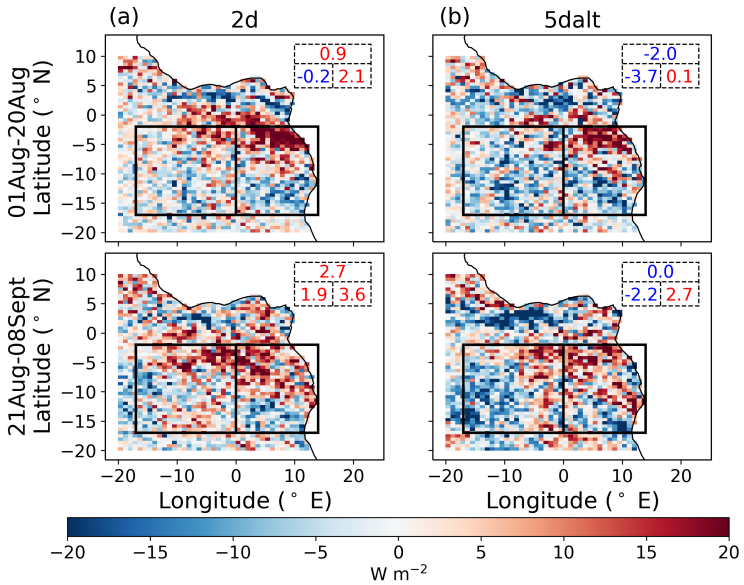

Figure S18: SDRE calculated according to Eq. (4), and averaged over the SEA from 01 Aug to 20 Aug (top row), and 21 Aug to 08 Sept (bottom row), 2017, for the 2d (a), and 5dalt (b) simulation sets. This is a companion plot to Fig. 16 in the main report. Values in the top right corner represent spatial averages of the overall (top), remote (left), and coastal (right) domains. Positive mean magnitudes are red for warming, and negative are blue for cooling.

8 Separating Shortwave and Longwave

Table S3: Longwave (LW) component REs (W m^{-2}) averaged over each domain from 01 Aug to 08 Sept 2017 for the DRE, IRE , and SDRE.

	Domain	**Nudged**	**1d**	**2d**	**5d**	**5dalt**	**Free Run**
LW DRE (W m^{-2}) from 01 Aug to 08 Sept	Coastal	0.03	0.03	0.03	0.04	0.04	0.03
	Remote	0.02	0.02	0.03	0.02	0.03	0.04
	Overall	0.02	0.02	0.03	0.03	0.04	0.03
LW IRE (W m^{-2}) from 01 Aug to 08 Sept	Coastal	-1.2	0.21	-0.02	-0.57	-0.60	-0.05
	Remote	-0.16	0.20	0.32	0.21	0.28	0.43
	Overall	-0.63	0.21	0.17	-0.14	-0.12	0.21
LW SDRE (W m^{-2}) from 01 Aug to 08 Sept	Coastal	3.0	0.10	1.2	1.9	2.1	4.8
	Remote	2.6	-0.02	0.71	1.6	1.4	2.3
	Overall	2.8	0.04	0.93	1.8	1.7	3.4